# Low-Energy Neutron Energy Spectra and the "Inverse Reaction" Cross Section*

G. R. Rao, B. L. Cohen, J. H. Degnan, and K. C. Chan
*University of Pittsburgh, Pittsburgh, Pennsylvania 15213*
(Received 2 August 1972)

A method is described for determining the 0–1.5-MeV part of the energy spectra of neutrons from $(p,n)$ reactions. It utilizes measurements of energy spectra of protons from $(p,np)$ reactions and corrections obtained by various measurements including neutron-proton coincidence studies. When the shapes of the neutron spectra are analyzed with the statistical theory, it is found that the cross section for the "inverse reaction" (capture of a low-energy neutron by a highly excited nucleus) exhibits a giant-resonance behavior as a function of mass number, peaking sharply near $A=91$. This peak is at least as sharp as is predicted by usual optical-model calculations.

## INTRODUCTION

One of the most important experiments for studying the statistical theory of nuclear reactions and for evaluating its parameters is the measurement of energy spectra from $(p, n)$ reactions. The low-energy part of these spectra are expected theoretically[1] to be represented by

$$N(E)=C\sigma_i E\exp(-E/T), \tag{1}$$

where $N(E)$ is the number of neutrons emitted with energy $E$, $C$ is a constant which is independent of neutron energy, $\sigma_i$ is the cross section for the inverse process (capture of the emitted neutron by the highly excited residual nucleus to form the compound nucleus), and $T$ is the nuclear temperature.[2] If $\sigma_i$ is weakly energy dependent, (1) is essentially a Maxwell distribution with the familiar rise to a peak at $E=T$ followed by an exponentially falling high-energy tail. Due to limitations in the experimental techniques, direct measurements[3,4] of neutron energy spectra have studied only this exponential tail.

A new technique capable of measuring the lower-energy portion of the spectrum was proposed recently.[5] It utilizes measurements of energy spectra of protons from $(p, np)$ reactions. It considers initially only cases where (a) the residual nucleus following a $(p, np)$ reaction is always left in its ground state. In such cases, the sum of the energies of the emitted neutron, $E_n$, and of the emitted proton, $E_p$, are equal to a constant, $E_0$, or

$$E_n=E_0-E_p, \tag{2}$$

where $E_0$ is equal to the energy of the incident proton plus the $Q$ of the reaction minus the energy of the recoiling residual nucleus. From (1) we see that a measurement of the energy distribution of the protons can be used to infer the energy distribution of the neutrons provided that (b) all $(p,n)$ reactions in which the neutron is emitted with an energy in the region of interest are followed by proton emission to give $(p, np)$ reactions; that is, $(p, n\gamma)$ is not a serious competitor; (c) the protons emitted from other reactions, like $(p, p'n)$ or $(p, p'\gamma)$, are subtracted off; and (d) $E_0$ is accurately known.

In Ref. 5, methods were presented for testing provisions a, b, c, and d, and one case, $^{90}$Zr, was found in which all of these provisions were satisfied. Some consideration was also given there to the possibility of modifying provision a to: (a′) the probability for the residual nucleus following a $(p, np)$ reaction to be left in its ground state is determined by some other means. One case of that type, $^{112}$Sn, was reported. In this paper we introduce another method for satisfying provision (a′), based on direct measurements of the probability for the nucleus to be left in its ground state. It is then used to determine energy spectra from $(p, n)$ reactions on two additional nuclei. The results, which are somewhat unexpected, are then interpreted as giving information on $\sigma_i$ in (1).

## EXPERIMENTAL METHOD AND RESULTS

The two nuclei found suitable for this study were $^{91}$Zr and $^{61}$Ni. Protons of different energies were obtained from the University of Pittsburgh three-stage Van de Graaff accelerator and were used to bombard self-supporting foils of $^{91}$Zr and $^{61}$Ni. The energy spectra of inelastically scattered protons were obtained with a charged-particle detector telescope consisting of a 50-$\mu$ $\Delta E$ detector, and a 2000-$\mu$ $E$ detector. Particle identification was done in the $E\times\Delta E$ mode. Typical energy spectra at different bombarding energies are shown in Fig. 1. The vertical lines indicate the highest outgoing proton energy for which a $(p, np)$ reaction is energetically possible. We shall refer to this en-

ergy as the $(p, np)$ threshold. Accurate energy calibration enabled the determination of the $(p, np)$ thresholds to within one half of one channel in Fig. 1. This was done by measuring elastic scattering at various bombarding energies and also by measuring deuterons from $(p, d)$ reactions on $^{91}$Zr and $^{61}$Ni at various bombarding energies. Since the $Q$ values for $(p, d)$ are higher than those for $(p, np)$ by the accurately known deuteron binding energy, the former were used to determine the $(p, np)$ thresholds accurately. In Fig. 1 we see that the contribution from $(p, np)$ seems to start a little before the threshold for $(p, np)$ reactions. This is probably due to poor energy resolution. Carbon- and oxygen-impurity peaks were easily subtracted off by comparison with spectra from Mylar targets. The dashed portions of the curves in Fig. 1 are the $(p, p')$ contributions to the spectra, and the way these were obtained is explained in the next paragraph.

The energy spectra at the different bombarding energies were plotted for the regions beyond and up to the $(p, np)$ thresholds. They were normalized to give the same intensity in the high $E_{p'}$ region. This was possible because there was very little variation with bombarding energy in the shape of the proton spectrum in this region. These curves are shown by the dashed lines in Fig. 1; they were used to estimate the $(p, p')$ contribution in the energy region where $(p, np)$ is present, under the assumption that if the shape of the $(p, p')$ spectrum beyond this region does not change with bombarding energy, it does not change in this region. For example, in Fig. 1(a) the region around $E_p' = 6$ MeV is the same relative to the region $E_p' > 7$ MeV for bombarding energies of 12.0 and 13.0 MeV, so we assume it is the same for a bombarding energy of 14.0 MeV. Although only three bombarding energies are shown in Fig. 1, several other intermediate and lower bombarding energies were used in obtaining the dashed curves in that figure. Proton energy spectra from $^{60}$Ni and $^{62}$Ni were also obtained at these energies. Here we do not have contributions from $(p, np)$ and we expect these spectra to closely resemble the $(p, p')$ spectra from $^{61}$Ni. The shape of the energy spectra were found to vary very little with bombarding energy and were very similar to the $(p, p')$ spectra from $^{61}$Ni, which serves as a check on the dashed curve in Fig. 1(b).

Neutron energy spectra obtained after subtraction of the $(p, p')$ contribution are shown by the solid curves for the different bombarding energies, in Fig. 2. The vertical lines indicate the thresholds for exciting the first excited state in the residual nucleus. The curves would represent the actual neutron energy spectra if (a) the residual nucleus is always left in the ground state; (b) every $(p, n)$ reaction is followed by proton emission

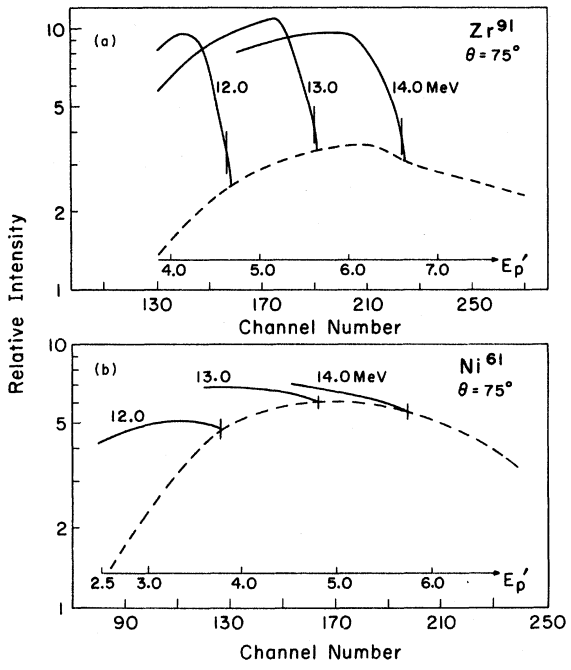


FIG. 1. Energy spectra in the region of interest at different bombarding energies for $^{61}$Ni and $^{91}$Zr. The spectra at the different energies have been normalized to give the same intensity in the high $E_p'$ region. The vertical lines indicate the $(p, np)$ thresholds.

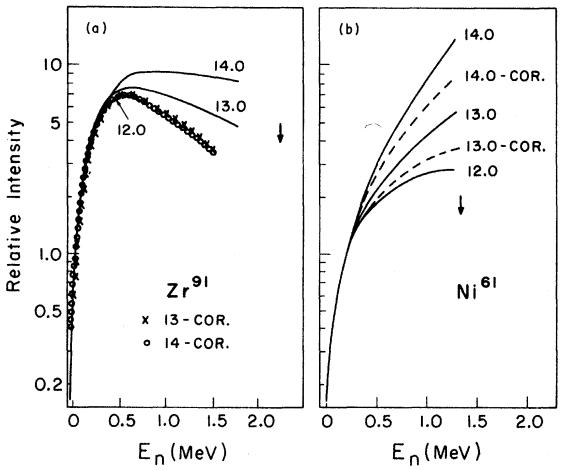


FIG. 2. Apparent neutron energy spectra at 12.0, 13.0, and 14.0 MeV incident energies, obtained after subtraction of the $(p, p')$ contribution. The arrows indicate the energies where the method breaks down because of contributions from $(p, np)$ leading to the first excited states. The dashed curves are the curves obtained by correcting with the factor $f$.

whenever it is energetically possible; i.e., $(p, n\gamma)$ and $(p, 2n)$ are not serious competitors.

We shall consider (b) first. The $Q$ values for $(p, 2n)$ reaction on $^{91}$Zr and $^{61}$Ni are −14.1 and −14.7 MeV, respectively; the bombarding energies used here were below the threshold for $(p, 2n)$ reactions. $\gamma$-ray competition becomes important only when the energy of the second proton is below about 3.5 MeV for $^{91}$Zr and 2.5 MeV for $^{61}$Ni.[5,6] For proton energies greater than these, and hence in the region of interest here, we may neglect $\gamma$-ray competition.

We shall now discuss (a), or rather, its substitute (a′). The residual nucleus may not always be left in its ground state and hence, correction for this must be made. Denote by $F$, the fraction of the time the residual nucleus is left in its ground state following a $(p, np)$ reaction. If $F$ is independent of neutron energy for a given bombarding energy, then the shape of the neutron spectrum for a given bombarding energy would remain unaltered. However, it was found for the cases studied that $F$ is a function of neutron energy and also of bombarding energy. Values of $F$ were directly measured by a neutron-proton coincidence experiment in which the neutrons were detected by time of flight in coincidence with the outgoing protons. The details of the experimental method were essentially the same as described by Cohen *et al.*[7] The excitation strength of the ground and excited states were measured as a function of neutron energy and these were used to determine $F$.

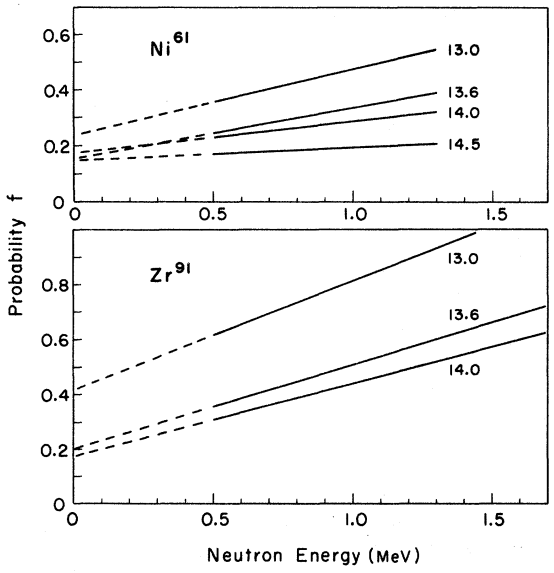


FIG. 3. The probability of exciting the ground state of the residual nucleus, $f$, as a function of neutron energy, for $^{91}$Zr and $^{61}$Ni, for different bombarding energies. Dashed lines show extrapolations from the measurements.

The results are shown in Fig. 3. Due to experimental limitations in the coincidence experiments, $F$ could not be determined for neutron energies below 0.5 MeV; values below that energy were obtained by extrapolation as shown by the dashed lines in Fig. 3. The values of $F$ from Fig. 3 were then used to correct the neutron energy spectra and obtain the dashed curves in Fig. 2. The data at 12 MeV has no correction since the excited states are not excited at such a low bombarding energy.

The probability of exciting the ground state of the residual nucleus, after a $(p, np)$ reaction was determined in the coincidence experiments, under the assumption that the contribution from $(p, pn)$ reactions is small compared to the contribution from $(p, np)$ reactions in those experiments. It is not possible to distinguish between $(p, pn)$ and $(p, np)$ reactions experimentally, and both contribute to the data used to obtain the probabilities. However, we can see from Fig. 1 that, for $^{91}$Zr, the ratio of $(p, np)$ to $(p, p')$ is about 3.5; and the $(p, p')$ background includes $(p, p'\gamma)$ as well as $(p, pn)$ reactions.[8] It is thus reasonable to hope that, for $^{91}$Zr, we may neglect the contribution of $(p, pn)$ in our determinations of $F$. A very satisfying confirmation of the validity of our procedure is that the neutron energy spectra obtained at 12.0-, 13.0- and 14.0-MeV bombarding energies, the dashed curves in Fig. 2(a), are in excellent agreement with one another even though the raw data before correction are quite different.

For $^{61}$Ni, the situation is not nearly so favorable. We see from Fig. 1(b) that the ratio of $(p, np)$ to $(p, p')$ is never larger than 0.35 and 1.0 at 14- and 13-MeV bombarding energies, respectively. We therefore expect contributions of $(p, pn)$ reactions

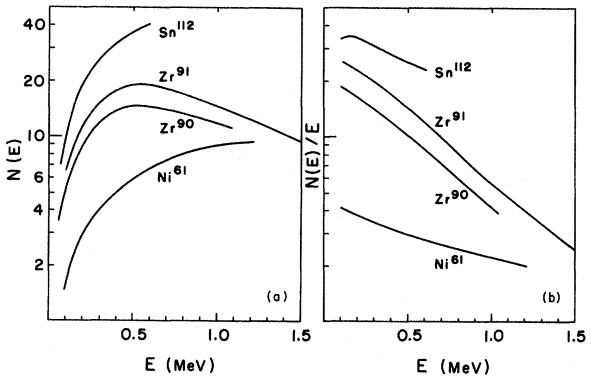


FIG. 4. (a) The final experimental results of this work. The results for $^{90}$Zr and $^{112}$Sn are obtained from previous work.[5] (b) Plots of $N(E)/E$ vs $E$ (neutron energy) for the four spectra in (a).

to be very important in the coincidence data used for the determination of $F$, especially at 14 MeV. This importance decreases appreciably at 13 MeV, and should be almost negligible at 12 MeV where the ratio of $(p, np)$ to $(p, p')$ is between 3 and 4 in the energy range of interest. [In the region corresponding to neutron energy below 1 MeV, the ratio of $(p, np)$ to $(p, p')$ is less, but it has been shown[8] that $(p, p')$ reactions giving protons in this energy region lead to $(p, p'\gamma)$ much more frequently than to $(p, pn)$, so contributions from $(p, pn)$ are not an important source of error here in the determination of $F$ from the coincidence data.] The actual neutron spectrum then should be not much different from the 13-MeV result in Fig. 2(b), and the 12-MeV result should be valid as it stands, since $F$ was found to be unity at that energy. The fact that the corrected curve for 13-MeV bombarding energy in Fig. 2(b) is not very different from the 12-MeV result corroborates the validity of the latter as the actual neutron spectrum.

The neutron spectra from $^{61}$Ni$(p, n)$ and $^{91}$Zr$(p, n)$ as derived above are shown in Fig. 4. They represent the final experimental results of this work. Also shown in Fig. 4 are the results of previous work on $^{90}$Zr and $^{112}$Sn,[4] and these four spectra exhibited in the more common form, $N(E)/E$.

## ANALYSIS OF RESULTS

In accordance with (1), a plot of $\log(N/\sigma_i E)$ vs $E$ should yield a straight line with a slope of $1/T$. Tests of this are shown in Fig. 5 for various assumptions about $\sigma_i$. One of these is the often used crude assumption that $\sigma_i$ is constant; it gives $T = 0.53$ MeV for $^{91}$Zr and $T = 1.55$ MeV for $^{61}$Ni. Two other calculations of $\sigma_i$ were obtained from the work of Auerbach and Perey.[9] One was done with the local optical-model parameters of Bjorklund and Fernbach[10] which gives $T = 0.84$ MeV for $^{91}$Zr and $T = 1.94$ MeV for $^{61}$Ni. The other used the more modern nonlocal optical-model potential of Perey and Buck[11] which gives $T = 0.65$ MeV for $^{91}$Zr and 1.6 MeV for $^{61}$Ni. In both of these optical-model potentials (see Table I) there is a rather steep rise in $\sigma_i$ at energies below 0.4 MeV which should cause a dropoff in the observed neutron energy spectrum, but no such dropoff was observed experimentally. This is the reason for the deviation of the data points below the straight lines in Fig. 5 for the optical-model potentials.

A much more serious discrepancy is the difference between the values of $T$ obtained in this analysis and those known from other sources. From the Gilbert-Cameron level densities[12] one calcu-

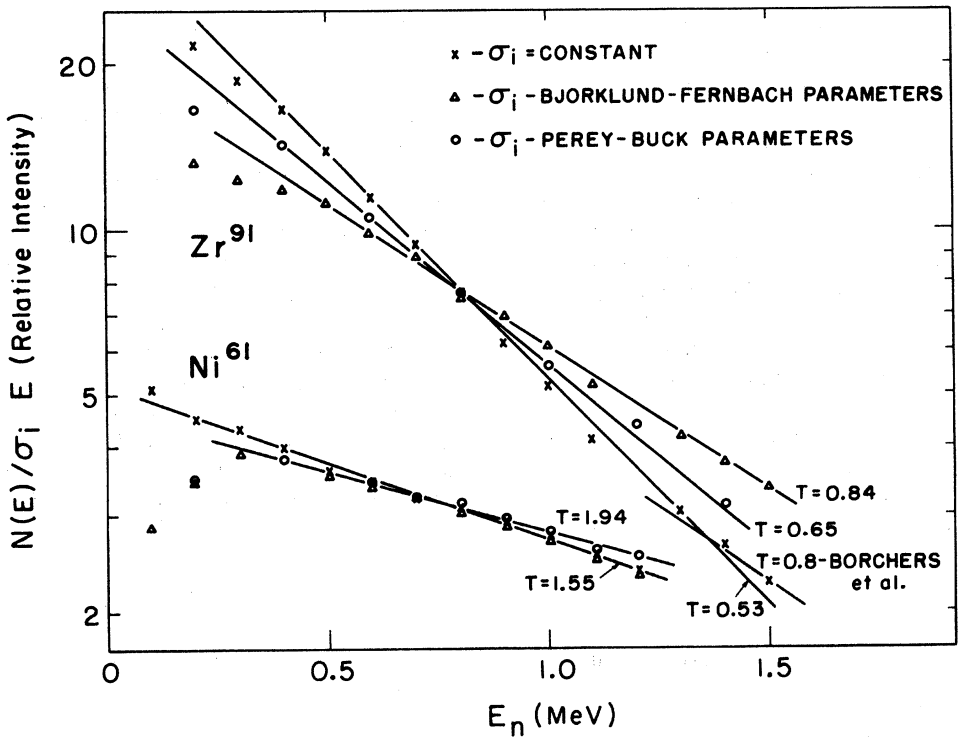


FIG. 5. Plots of $[N(E)]/(\sigma\ E)$ vs $E$ for $^{61}$Ni and $^{91}$Zr with $\sigma$ obtained in different ways. The points indicate the experimental data while the straight lines are drawn for different values of $T$ in (1).

TABLE I. Optical-model parameters used in Ref. 9.

| | Local Bjorklund-Fernbach | Nonlocal Perey-Buck | Equivalent local at 4.1 MeV Perey-Buck |
|---|---|---|---|
| $V_0$ | 50.0 MeV | 70.0 MeV | 41.35 MeV |
| $W_0$ | 7.0 MeV | 7.0 MeV | 3.95 MeV |
| $V_{so}$ | 9.5 MeV | 7.2 MeV | 7.2 MeV |
| $r_0$ | 1.25 fm | 1.25 fm | 1.32 fm |
| $a$ | 0.65 fm | 0.65 fm | 0.62 fm |
| $b$ | 0.98 fm | 0.65 fm | 0.65 fm |
| $\beta$ | ... | 1.00 fm | ... |

lates $T = 1.0$ MeV for $^{91}$Zr and 1.05 MeV for $^{61}$Ni. Direct measurements of neutron spectra in the higher energy region where the effects of $\sigma_i$ are not important give $T \simeq 1.0$ MeV for nuclei in the region of $^{7}$Zr and $T \simeq 1.15$ MeV for nuclei in the Ni region.[4] Thus the slopes in Fig. 4 are too steep for $^{91}$Zr and not nearly steep enough for $^{61}$Ni. The simplest explanation for these discrepancies is that none of the calculations of $\sigma_i$ are sufficiently accurate. Further light on this interpretation can be obtained if we consider the ratio of $\sigma_i$ at the highest and lowest energies at which the experimental data are most reliable, say 1.2 and 0.5 MeV. This ratio for the two optical-model potentials is plotted vs $A$ in Fig. 6. Experimental values for this ratio may be obtained from Fig. 4 if we assume that the true temperatures are 1.0 MeV for Zr and 1.15 MeV for Ni as indicated above, and that the difference between the observed spectra and a simple Maxwell distribution with these temperatures is caused by the $\sigma_i$ term in (1). The values of $\sigma_i(0.5\ \text{MeV})/\sigma_i(1.2\ \text{MeV})$ obtained by this procedure are shown by the crosses in Fig. 6. The ratio for $^{90}$Zr is included; it differs from the $^{91}$Zr ratio because $Q(p, n)$ is more negative for $^{90}$Zr whence $T$ is expected to be lower. A point in Fig. 6 is also shown for $^{112}$Sn, based on a large extrapolation of the data in Fig. 4; it should be considered as only qualitatively accurate, although it is clear from Fig. 4 that this point must lie much lower than the ones for Zr.

From Fig. 6 we see that the resonance behavior of $\sigma_i$ predicted by the optical-model potentials is very much in evidence; in fact the experiments suggest a stronger and sharper resonance than is

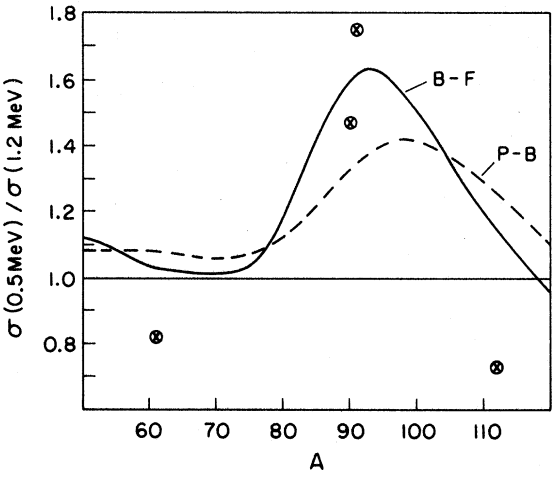


FIG. 6. The curves show the ratio of $\sigma_i(0.5\ \text{MeV})$ to $\sigma_i(1.2\ \text{MeV})$ for the Bjorklund-Fernbach (marked B-F) and the Perey-Buck (marked P-B) parameters, plotted as a function of mass number $A$. The points are the experimentally obtained values for $^{61}$Ni, $^{90}$Zr, $^{91}$Zr, and $^{112}$Sn.

predicted by the theory. The position of the resonance is better predicted by the Bjorkland-Fernbach potential than by the Perey-Buck. It would be interesting to have calculations performed with some of the more recent optical-model analyses which include isospin dependence. This would enable the use for neutrons of the large amount of proton data.

It should be noted that the optical-model potentials were designed to calculate reaction cross sections for nuclei in their ground states, whereas the experiments here determine reaction cross sections on nuclei in states at 8–12 MeV excitation energy. If anything, one would expect the excitation energy to lead to an increase in the imaginary potential, $W$, which then would spread the resonance and make it less sharp. Such does not seem to be the case here; these effects presumably do not arise until the excitation energy becomes much higher. Another effect on which there has been speculation is the possibility that nuclear sizes change appreciably with excitation energy. The data here are not sufficiently detailed to detect such an effect.

*Work supported by the National Science Foundation.

[1]J. M. Blatt and V. F. Weisskopf, in *Theoretical Nuclear Physics* (Wiley, New York, 1952).

[2]Actually the $1/T$ in the exponent of (1) is the first term of a series in which the second term is smaller than the first by the factor $E/4E_0$. For cases in which we use (1) here, $E \sim 1$ MeV, $E_0 \sim 10$ MeV, so this approximation is quite accurate, but it is clear that (1) cannot be used when $E$ approaches $E_0$.

[3]R. R. Borchers, R. M. Wood, and C. H. Holbrow, Nucl. Phys. 88, 689 (1966); R. M. Wood, R. R. Borchers, and H. H. Barschall, *ibid.* 71, 529 (1965).

[4]S. M. Grimes, J. D. Anderson, J. W. McClure, B. A. Pohl, and C. Wong, Phys. Rev. C 3, 645 (1971); C 4, 607 (1971).
[5]B. L. Cohen, J. H. Degnan, C. L. Fink, G. R. Rao, and R. Balasubramanian, Phys. Rev. Letters 26, 23 (1971).
[6]C. L. Fink and B. L. Cohen, Phys. Rev. (to be published).
[7]B. L. Cohen, E. C. May, T. M. O'Keefe, and C. L. Fink, Phys. Rev. 179, 962 (1969).
[8]B. L. Cohen, E. C. May, T. M. O'Keefe, C. L. Fink, and B. Rosner, Phys. Rev. Letters 21, 226 (1968).
[9]E. H. Auerbach and F. G. J. Perey, Brookhaven National Laboratory Report No. BNL 765 (T-286), 1962 (unpublished).
[10]F. Bjorklund and S. Fernbach, Phys. Rev. 109, 1296 (1958).
[11]F. Perey and B. Buck, Nucl. Phys. 32, 353 (1962).
[12]A. Gilbert and A. G. W. Cameron, Can. J. Phys. 43, 1446 (1965).

PHYSICAL REVIEW C VOLUME 7, NUMBER 2 FEBRUARY 1973

# Multipole Mixing Ratios for Selected Transitions in $^{154}$Gd

D. R. Ober, W. Weeber, and R. L. Place
*Department of Physics, Ball State University, Muncie, Indiana 47306*
(Received 22 May 1972)

$\gamma$-ray mixing ratios have been measured for four transitions in $^{154}$Gd. The mixing ratios were obtained through the analysis of $\gamma$-ray angular correlations involving the transitions in question. All cascades had the $2^-$ octupole level at 1719.6 keV as the initial emitting state. A Ge(Li)-NaI(Tl) detector array was used to measure correlations for the following cascades: 592-1005 keV ($2^-$-$3^+_\gamma$-$2^+_{g.s.}$); 723-996 keV ($2^-$-$2^+_\gamma$-$0^+_{g.s.}$); 723-873 keV ($2^-$-$2^+_\gamma$-$2^+_{g.s.}$). A two-parameter $[\delta(\gamma_1), \delta(\gamma_2)]$ search routine was developed for the analysis of the correlations involving two mixed-multipole transitions. Results for the mixing ratios are: $\delta(592) = 0.08^{+0.14}_{-0.22}$; $\delta(723) = 0.04^{+0.02}_{-0.04}$; $\delta(873) = -10.0^{+2.0}_{-4.0}$; $\delta(1005) = -9.5^{+7}_{-4}$.

In this article we report mixing ratios for several transitions in $^{154}$Gd. The mixing ratios were obtained from angular-correlation data taken between $\gamma$ rays in the 592-1005-, 723-996-, and 723-873-keV cascades. In each case the initial state is the $2^-$ octupole state at 1720 keV. The intermediate states are $2^+$ and $3^+$ members of the $\gamma$ band. Figure 1 shows the pertinent part of the $^{154}$Gd energy level scheme. A more complete level scheme can be found in the article by Meyer.[1]

The mixing ratio for the 1005-keV transition has previously been measured by several investigators[2-5] with agreement between the values of Rud and Nielsen[3] and Lange *et al.*[5] In the present report the correlation between the 592-keV and 1005-keV $\gamma$ rays is used to obtain mixing ratios for both the 592- and 1005-keV transitions. Previously the 592-keV transition was assumed to be pure $E1$.[3] The possibility of sizable $M2$ contributions in transitions from the $2^-$ octupole state is of interest, since large $M2$ as well as $E3$ contributions have been reported in similar transitions for nuclei around $A = 180$. We have also measured the mixing ratios for the 723- and 873-keV transitions, and these are included in this report.

The $^{154}$Eu sample[6] was in the form of $^{154}EuCl_3$ in 1 *N* HCl solution. A source for the correlation work was prepared by depositing a small amount of the solution in a thin-wall (0.3-mm) capillary tube. The source was centered in the angular-correlation system to within 1% as determined by the singles count in a movable detector.

All correlations were measured between a Ge(Li) and either one or three NaI(Tl) detectors. Two different Ge(Li) detectors, both ORTEC true coaxial, were used during the experiment. Resolutions for these detectors at 1330 keV were 3.3 and 2.1 keV. The active volume in each Ge(Li) detector was about 30 cm$^3$. The NaI(Tl) detectors were 7.62 cm$\times$7.62 cm.

Real-plus-accidental coincidences and purely accidental coincidences for a selected portion of the Ge(Li) spectrum were concurrently accumulated and stored in separate portions of the multichannel analyzer (MCA) memory. A block diagram of the electronics arrangement used in the multidetector system is shown in Fig. 2.

The multidetector configuration utilizes a modified fast-slow coincidence system. Timing signals from the Ge(Li) detector were derived using an ORTEC 453 constant-fraction-timing discriminator (CFTD) preceded by an ORTEC 454 timing-filter amplifier. The CFTD output was presented to one side of the fast-coincidence circuit. Energy-discriminated timing signals from the NaI(Tl) side were presented to the fast-coincidence circuit by